RESEARCH PAPER
Contrib. Sci. & Tech Eng, 2026, 3(1)
Homepage: https://cste.journals.umz.ac.ir/
DOI: 10.22080/cste.2025.29838.1074

Seismic Assessment of the Concrete Buttress Dam Using Three-Dimensional Finite Element Analysis

Seyyed Meisam Aghajanzadeh [1]*, Hasan Mirzabozorg [2]

[1] *Assistant Professor, Department of Civil Engineering, Faculty of Engineering and Technology, University of Mazandaran, Babolsar, Iran.*

[2] *Associate Professor, Department of Civil Engineering, K. N. Toosi University of Technology, Tehran, Iran.*

Article Info
Received 12 August 2025
Accepted 30 October 2025
Available online 12 February 2026

Keywords:
Concrete Buttress Dam;
3-D Finite Element Modeling (FEM);
Dynamic Response;
Dam–Foundation–Reservoir Interaction.

Abstract:

This study investigates the structural performance of a concrete buttress dam under static and seismic loading, with a focus on dam–foundation–reservoir interaction. A three-dimensional finite element model was developed using the available geometric, material, and geological data to assess the stress distribution, displacement patterns, and dynamic responses under critical load combinations. Material properties were determined from the assumed values and established empirical relationships, accounting for differences between static and dynamic conditions. Seismic performance was evaluated for Design Basis Level (DBL) and Maximum Credible Level (MCL) scenarios using site-specific ground motion records. Results show that the tensile and compressive stresses are localized and remain below the concrete's capacity. The maximum crest displacement under MCL loading was 13.0 mm, which is within acceptable safety limits. Overall, the findings indicate that the analyzed configuration maintains sufficient safety margins against cracking, crushing, and excessive deformation, providing a robust technical foundation for the planned capacity-enhancement measures.

***Corresponding Author:** s.m.aghajanzadeh@umz.ac.ir

Supplementary information: Supplementary information for this article is available at https://cste.journals.umz.ac.ir/

Please cite this paper as: Aghajanzadeh, S. M. , & Mirzabozorg, H. (2026). Seismic Assessment of the Concrete Buttress Dam Using Three-Dimensional Finite Element Analysis. Contributions of Science and Technology for Engineering, 3(1), 41-51. doi:10.22080/cste.2025.29838.1074.

1. Introduction

Reliable water storage is essential for economic development, food security, and sustainable water management. Various structural systems are used to store water, ranging from elevated tanks to large reservoir dams, each requiring appropriate design and safety evaluation. Recent research has highlighted the importance of accurately assessing the seismic behavior of such storage structures and their interaction with contained water [1-3]. Among these systems, large dams play a particularly critical role in regulating river flows, supplying water for municipal and agricultural use, generating hydropower, and mitigating floods [4]. With increasing population pressures and climate variability, the performance and resilience of existing dams have become matters of growing importance. Many aging structures now face capacity constraints and evolving safety requirements, necessitating rehabilitation and modification projects [5-7]. Crest heightening is a common and effective strategy to enhance dam functionality, substantially increasing storage capacity and operational flexibility. However, such modifications alter the structural and hydraulic behavior of the dam–foundation–reservoir system, requiring rigorous engineering assessment to ensure long-term stability and compliance with modern safety standards [8, 9].

Numerous studies have examined the structural behavior of dams subjected to modifications such as heightening, spillway expansion, or seismic retrofitting [10]. The Mauvoisin Dam in Switzerland was raised by 13.5 m, adding 29 million m³ of storage and 100 GWh of seasonal output, with monitoring confirming stable performance [11]. To improve seismic safety, Wieland (2004) [12] proposed strategies including crest thickening, geometric modifications, post-tensioning, seismic belts, and shear keys. Fu et al. (2011) [13] demonstrated, using 3D FEM, that problems in arch dam heightening—such as increased heel stress, cracking, and poor bonding—can be mitigated through targeted construction and temperature-control measures. Advanced computational approaches have also been applied: Chen et al. (2019) [14] used an ICS-IPSO inversion method to identify realistic elasticity distributions for FEM safety assessments, while Chen et al. (2021) [15] introduced a deformation early-warning index for heightened gravity dams, effective for real-time evaluation. At a system scale, Clerc et al. (2021) [16] assessed the Grande Dixence Dam in Switzerland. They concluded that

*ISSN **3060-6578***

moderate crest elevations (10–15 m) can meet design and economic requirements while imposing limited environmental impacts.

When a dam is heightened or strengthened, its structural behavior undergoes significant changes, and external loads, such as reservoir water levels, may reach unprecedented magnitudes, making it essential to accurately characterize dam behavior and rigorously assess its structural state [16-20]. To address this need, the finite element method can be employed to simulate the complex interactions between the dam body, foundation, and reservoir, thereby enabling a comprehensive evaluation of stress distributions, deformation patterns, and potential failure modes under both operational and extreme loading conditions [21-23]. Building on finite element capabilities, various researchers have developed specialized approaches to enhance the accuracy and applicability of dam safety assessments. Karimi et al. (2010) [24] used a coupled finite element, boundary element model to generate training data for an artificial neural network. Zhang et al. (2013) [25] used the extended finite element method to model seismic crack initiation and propagation in gravity dams, demonstrating its effectiveness for reliable seismic safety evaluation. Løkke and Chopra (2019) [26] developed a direct finite element method that fully couples the dam–reservoir–foundation system, incorporating material nonlinearity, contact behavior, and hydrodynamic effects in the time domain.

Beyond computational methodologies, the structural typology of a dam strongly influences both analysis and the choice of remedial measures. This study focuses on a concrete buttress dam, a type that has also been widely investigated [27]. Enzell et al. (2023) [28] performed large-scale physical tests on a 1:15 scale, five-monolith buttress dam model, showing that increased lateral restraint and shear transfer improve stability but can enlarge breach size. Their findings challenge the common assumption of single-monolith failure and underline the importance of 3D effects in stability analyses. Abbasiverki et al. (2021) [29] used 3D nonlinear FEM to study seismic behavior under high-frequency excitations, including cross-stream vibrations and topographic amplification. They demonstrated that the slender geometry of buttress dams makes them highly sensitive to such motions and that simplified foundation models, particularly the massless method, can yield unreliable predictions, reinforcing the need for accurate dam–reservoir–foundation interaction modeling.

In summary, the literature demonstrates important advances in the analysis and safety assessment of concrete dams, but relatively few studies have focused specifically on buttress dams subjected to heightening. The unique structural configuration of these dams, combined with the changes introduced by crest elevation, requires a dedicated assessment approach. The present study addresses this gap by investigating the static and seismic behavior of a heightened buttress dam using three-dimensional finite element modeling. The model explicitly incorporates dam–foundation–reservoir interaction and evaluates performance under two seismic hazard levels: the Design Basis Level (DBL) and the Maximum Credible Level (MCL). Stress distribution, displacement behavior, and dynamic response under critical load combinations were assessed. The outcomes verify the modified dam's structural integrity and provide a technical basis for evaluating the feasibility and safety of the capacity-enhancement modifications.

2. Buttress Dam

A concrete buttress structure with a maximum height of 53.8 m and a crest length of 286 m is considered. The upstream and downstream slopes are 0.45:1 and 0.70:1 (V:H), respectively. Figure 1 presents a simplified geometric representation of a dam, divided into 10 distinct zones to facilitate analysis of stress, displacement, and dynamic response. However, it does not represent a traditional finite element model with a mesh. Zone 1 is situated near the upper upstream side, while Zone 2 lies slightly below it along the upstream face, which is also represented by Zone 9. Zone 3 is positioned near the heel, corresponding to Zone 10, and Zone 4 is located near the downstream toe, alongside Zones 5 and 6, which specifically denote the toe regions. Zones 7 and 8 capture the transition areas between the original structure and its modified portion. The green section represents a proposed addition to the dam, designed to enhance its capacity and provide a consistent framework for evaluating and comparing the dam's behavior across various load combinations and excitation levels.

2.1. Concrete Properties

Elastic properties for static and dynamic analyses are shown in Table 1. For the dynamic analysis, these values were increased by 25% to account for the higher stiffness that concrete typically exhibits under seismic loading due to strain-rate effects [8]. This adjustment allows the model to capture more realistically the stiffer response of the dam body during earthquake excitation. No increase was applied to the filler concrete, as it forms part of the foundation.

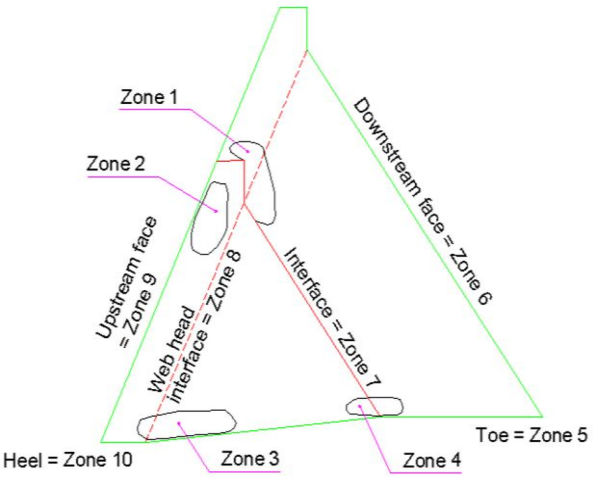

Figure 1. Zoning of the dam body Materials Properties

Table 1. Elastic Properties of Concrete for Static and Dynamic Analysis

Material	Elastic Modulus (GPa)	Poisson's Ratio	Shear Modulus (GPa)	Density (kg/m³)	Thermal Expansion Coefficient (×10⁻⁶/°C)
Existing dam concrete	30 (37.5*)	0.17 (0.17*)	12.82 (16.025*)	2400	9.0×10^{-6}
Added-section concrete	20 (25*)	0.17 (0.17*)	8.55 (10.69*)	2400	9.0×10^{-6}
Filler concrete	9.06 (9.06)	0.18 (0.18)	3.82 (3.82)	–	–

*Values in parentheses are for dynamic analysis.

The concrete in the existing dam has a 90-day cube compressive strength of 40 MPa, as reported in Table 2. For the dynamic analysis, this strength was increased by 30%, giving a design value of 52 MPa. This adjustment reflects the strain-rate effect, where concrete typically shows higher strength under seismic loading compared with static conditions. The adopted 30% increase provides a practical representation of the material's enhanced resistance under earthquake excitation. The tensile strength is 5 MPa. For the concrete in the newly added section, the tensile strength was calculated using the empirical relationship proposed by Raphael:

$$f_t = 0.32 f_c'^{2/3} \quad (1)$$

where f_t is the direct tensile strength of concrete (MPa) and f_c' is the uniaxial compressive strength of concrete (MPa). This widely used formulation provides realistic estimates of tensile strength when direct measurements are unavailable. Following standard engineering practice, the true tensile strengths derived from this relationship for static and dynamic conditions were adopted in the analysis, and based on the assumed compressive strength, application of the Raphael equation yielded tensile strengths of 3.74 MPa for static loading and 5.79 MPa for dynamic loading, which were subsequently used in the finite element analyses. The shear strength at the joint between the existing dam and the added section, determined using the Stucky empirical formula, was approximately 1 MPa without considering reinforcement, with potential for enhancement through strengthening measures. The required compressive strength for the added section was assessed using the Kupfer biaxial failure envelope for conventional structural concrete, applying safety factors of 3.0 for compression–compression and 1.0 for tension–tension under static loading.

The elastic properties of the various foundation materials used in the analysis are presented in Table 2. It should be noted that, for the dynamic analyses, no increase was applied to the elastic modulus or shear modulus of the foundation materials.

Table 2. Elastic Properties of Foundation Materials

Material	Elastic Modulus (GPa)	Poisson's Ratio	Shear Modulus (GPa)
Black schist marl	8.6	0.30	2.63
Fault zone	5.0	0.35	1.85
Limestone	11.9	0.25	6.13

3. Loading

3.1. Static Loading

The static loading conditions considered for the dam comprise the structure's self-weight, hydrostatic pressure, and thermal effects. In accordance with the findings of previous studies, the effects of sediment deposition, flood loading, and ice pressure were deemed negligible and therefore excluded from the analysis. The influence of uplift pressure, corresponding to a full-reservoir condition, on the distribution of tensile and compressive stresses within the dam body is illustrated in Figures 2 and 3. As evidenced by the results, the magnitude of stresses induced by uplift is extremely small, approximately 0.03 MPa in both tension and compression; consequently, uplift pressure was omitted from the final static load combinations.

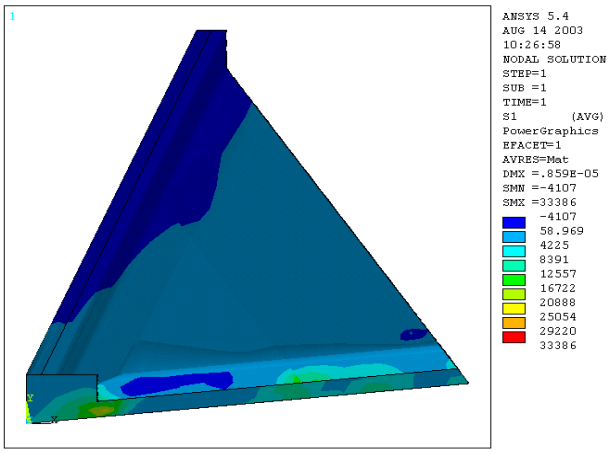

Figure 2. Tensile stresses in the dam structure due to uplift pressure under full-reservoir conditions

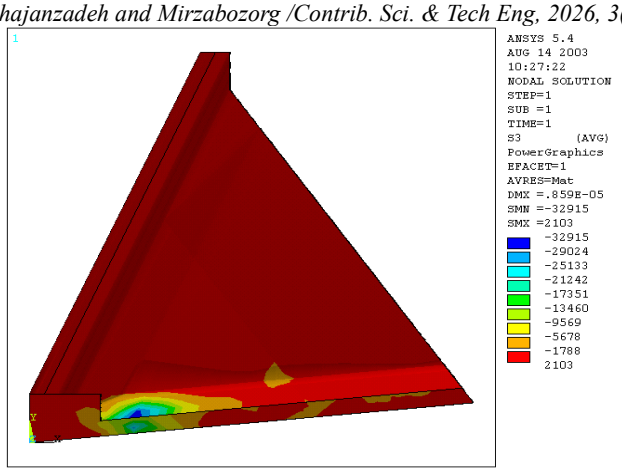

Figure 3. **Compressive stresses in the dam structure due to uplift pressure under full-reservoir conditions**

Self-weight represents the weight of the dam body, with the foundation considered massless. For the analysis, the unit weight of concrete was taken as 2400 kg/m³. Hydrostatic pressure acts on the upstream face of the dam as well as on the foundation. Since the reservoir was not to be emptied during the construction of the added section, the hydrostatic load was also applied in stages. A three-dimensional steady-state thermal analysis was carried out for two temperature-loading scenarios, representing summer and winter conditions, applied to the dam body. The maximum and minimum ambient temperatures at the site are 22.5 °C and 0 °C, respectively. Given that the upstream face of the dam is oriented to the south, solar radiation effects were accounted for, based on the recommendations of the Stucky reports, by increasing the summer and winter air temperatures by 2 °C and 5 °C, respectively. Due to limited available data on the reference temperature of the concrete and its influence on the analysis results, two reference temperatures were considered: 0 °C and the mean annual air temperature of 11.25 °C. For the empty-reservoir condition in winter, the temperature of the upstream face was taken as 5 °C, while the temperature of all other faces was assumed to be 0 °C.

3.2. Dynamic Loading

For the dynamic loading evaluation, two seismic performance levels were adopted: the Design Basis Level (DBL) and the Maximum Credible Level (MCL). The DBL corresponds to an earthquake during which the dam must retain full structural functionality with no significant damage under the associated peak accelerations. The MCL represents the most severe earthquake considered credible for the site, under which the dam may experience limited and repairable damage but without compromising overall stability or safety. Site-specific seismic hazard studies were used to define the peak ground accelerations (PGA) for both horizontal and vertical components at each level, as presented in Table 3. The earthquake records selected for the analysis are listed in Table 4, and each record was scaled to match the target PGA values for DBL and MCL. The dynamic load combinations considered are summarized in Table 5 and were applied for both seismic levels.

Table 3. **Peak Ground Accelerations for DBL and MCL Earthquake Levels**

Earthquake Level	Peak Horizontal Acceleration (g)	Peak Vertical Acceleration (g)
DBL	0.17	0.12
MCL	0.38	0.22

Table 4. **Earthquake Records Used in Dynamic Analyses**

Earthquake Level	Earthquake Name	Event Date	Recording Station
DBL	Cal-Teck	9 February 1971	San Fernando
DBL	San Rocco	15 September 1976	Friuli–Italy
MCL	Imperial Valley	15 October 1979	Compuertas
MCL	Manjil	20 June 1990	Abbar

Table 5. **Dynamic Load Combinations**

Combination	Self-weight	Hydrostatic Pressure at Initial Dam Crest Level	Hydrostatic Pressure at Heightened Dam Crest Level	Summer Temperature	Winter Temperature	Earthquake
1	×	×		×		×
2	×	×			×	×
3	×		×	×		×
4	×		×		×	×
5	×			×	×	×

4. Finite Element Modeling

For the modeling, meshing, and analysis of the dam, foundation, and reservoir system, ANSYS 5.4 software was employed. The dam body and foundation were primarily meshed with SOLID45 elements, eight-node brick elements with three translational degrees of freedom per node. In certain areas of the dam body and foundation where geometric complexity existed, wedge-shaped SOLID45 elements were used. To account for the influence of the foundation on the structural response, a massless foundation model with dimensions approximately twice those of the dam in each direction was adopted [30], with all outer boundary nodes except those on the top surface fully restrained. Damping ratios of 5% and 10% were assigned for the DBL and MCL earthquake levels, respectively. The thermal analysis of the dam body was performed using SOLID70 elements, eight-node units with a single thermal degree of freedom, geometrically consistent with the SOLID45 elements. Hydrostatic and hydrodynamic effects from the reservoir were modeled with FLUID30 elements, each having three translational and one pressure degree of freedom per node, with zero pressure at the free surface and energy-absorbing boundaries applied to prevent wave reflection. Bottom wave absorption was conservatively set at 20% following FERC guidelines and Chopra's formulations. Figure 4 shows the finite element models of the dam–reservoir–foundation system, comprising 1,329, 2,162, 3,241, and 480 elements, respectively.

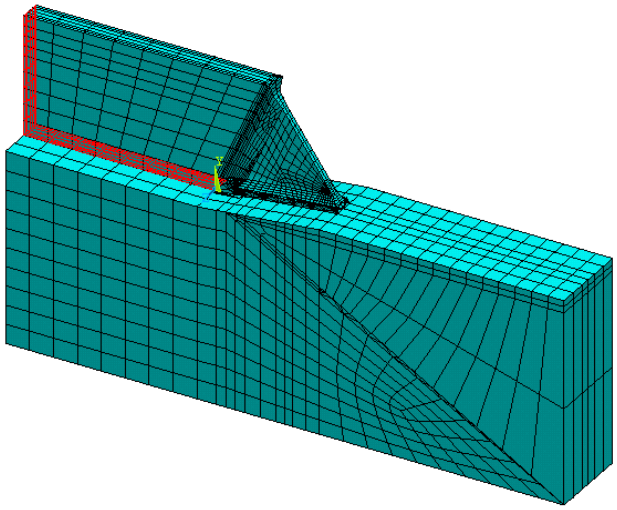

Figure 4. Three-dimensional finite element model of the complete dam–reservoir–foundation system

4.1. Boundary Conditions in Dynamic Analysis

Since only a single block was modeled, it was necessary in the dynamic analysis (for accelerations parallel to the dam axis) to account for the effective lateral stiffness provided by adjacent blocks. This stiffness can range from a full restraint condition, where adjacent nodes are completely tied together in the parallel direction, to a completely free condition, where nodes are only connected within the foundation. Between these extremes, two intermediate cases were also examined: Local Restraint 1, where nodes are tied within the foundation and the lower one-third of the dam height, and Local Restraint 2, which extends these ties to include nodes near the crest as well. The full restraint case represents a conservative assumption in the direction of safety (overly stiff), while the completely free case represents the opposite extreme, an overly flexible and highly conservative assumption in terms of deformation. To evaluate these effects, a sensitivity analysis was performed for the third dynamic load combination under MCE-level excitation (Manjil earthquake). The results, summarized in Table 6, indicate that Local Restraint 2 provides the most realistic balance; therefore, this configuration was adopted for the final dynamic analyses.

Table 6. Sensitivity Analysis for Determining Appropriate Lateral Stiffness

Analysis Case	Mode 1 (Hz)	Mode 2 (Hz)	Mode 3 (Hz)	Max. Tensile Stress – Zone 4 (MPa)	Max. Tensile Stress – Zone 6 (MPa)	Max. Tensile Stress – Zones 2 & 9 (MPa)
Full restraint	5.2805	6.7174	11.5960	2.35	2.86	4.86
Free	1.2929	4.4229	6.7072	3.24	2.21	9.62
Local restraint 1	2.1681	4.6135	6.7131	2.59	2.34	9.65
Local restraint 2	4.3629	6.7131	9.1510	2.50	2.98	4.84

The sensitivity analysis demonstrates that Local Restraint 2 provides a realistic balance between the overly rigid full restraint and the overly flexible free case. For example, Mode 1 frequency under Local Restraint 2 (4.36 Hz) lies between the full restraint (5.28 Hz) and free case (1.29 Hz), indicating an appropriate representation of the effective lateral stiffness contributed by adjacent monoliths. Similarly, tensile stress results remain moderate, avoiding

the unrealistically high concentrations of the free case while not underestimating them as in the full restraint case. These outcomes confirm that Local Restraint 2 captures the structural interaction most accurately and was therefore adopted as the representative boundary condition in the final dynamic analyses.

5. Results

This section presents the results of the dynamic analyses conducted with simultaneous seismic excitation applied in all three orthogonal directions for both the Design Basis Level (DBL) and Maximum Credible Level (MCL) hazard levels. The earthquake ground motion records utilized, along with the corresponding dynamic load combinations, are detailed in Table 5. The results for the DBL hazard level are summarized in Table 7, which presents the maximum tensile and compressive stresses, their respective locations, and the corresponding required compressive strengths for each load combination.

Table 7. Results of Various Dynamic Load Combinations under DBL Excitation

Dynamic load combination	Maximum compressive stress (MPa)				Maximum tensile stress (MPa)			
	Existing dam	Added section	Existing dam	Added section	Existing dam	Added section	Existing dam	Added section
Load Combination 1 (t_ref = 11.25°C)	4.38	5.15	Zone 4	Zone 5 and 6	3.66	1.95	1/3 height of upstream face	Zone 9
Load Combination 2 (t_ref = 11.25°C)	4.88	3.62	Zone 4	Upstream face, Zone 9	3.81	2.47	1/3 height of upstream face	Zones 5 & 6
Load Combination 3 (t_ref = 11.25°C)	7.20	7.20	Zone 4	Zones 5 & 6	5.22	3.11	1/3 height of upstream face	At connection of upstream face
Load Combination 4 (t_ref = 11.25°C)	6.57	4.93	Zone 4	Zone 4	3.89	2.66	1/3 height of upstream face	Near crest
Load Combination 5 (t_ref = 11.25°C)	3.49	3.61	Zone 4	Zone 6 (local)	6.83	5.99	Zones 3 & 4 (local)	Zones 4 & 5 (local)

Table 7 demonstrates that both tensile and compressive stresses under DBL excitation remain within relatively limited ranges. High tensile stresses in the third and fifth load combinations are confined to small regions near the upper upstream face and are primarily due to boundary constraints; these effects are localized and not structurally significant. Compressive stresses are similarly modest, with the maximum value of 7.2 MPa occurring in the third load combination within Zone 4. Building on these observations, the subsequent analysis for the MCL excitation level, summarizing the corresponding maximum tensile and compressive stresses and their locations, is presented in Table 8.

Table 8. Results of Various Dynamic Load Combinations under MCL Excitation

Dynamic load combination	Maximum compressive stress (MPa)				Maximum tensile stress (MPa)			
	Existing dam	Added section	Existing dam	Added section	Existing dam	Added section	Existing dam	Added section
Load combination 1 (t_ref = 11.25°C)	5.73	6.41	Zone 4	Zone 5 and 6	4.11	3.11	1/3 height of upstream face	Zones 9 and 5
Load combination 2 (t_ref = 11.25°C)	6.59	5.26	Zone 4	Zone 4	4.95	5.16	1/3 height of upstream face	Zones 5 and 6
Load combination 3 (t_ref = 11.25°C)	8.76	9.54	Zone 4	Zones 5 and 6	6.148	4.10	1/3 height of upstream face	At connection of upstream face
Load combination 4 (t_ref = 11.25°C)	8.88	7.25	Zone 4	Zone 9	5.20	4.44	1/3 height of upstream face	Zones 5 and 6
Load combination 5 (t_ref = 11.25°C)	4.82	4.45	Zone 4	Zone 6 (local)	7.08	6.24	Zones 3 and 4 (local)	Zones 4 and 5 (local)

In the added section, the maximum tensile stress (5.16 MPa, Load Combination 2) occurs near the downstream buttress end due to geometric discontinuities, while surrounding areas remain at much lower stress levels (Figure 5). In Load Combination 5, the maximum tensile stress rises to 6.24 MPa near the buttress extremity (Figure 6), but the affected zone is minimal and not a global structural concern. Across the remainder of the dam body, tensile stresses remain well below critical thresholds, suggesting that the structural integrity is not compromised under these combinations. The spatial distributions in both cases indicate that localized tensile peaks are primarily driven by geometry-induced stress concentrations and boundary-condition effects, rather than by widespread material overstressing.

Under Load Combination 4, the existing dam shows a maximum compressive stress of 8.88 MPa (Figure 7), concentrated near the buttress base and upstream crest where hydrostatic and seismic loads overlap. The majority of the structure exhibits significantly lower compressive stresses, indicating that the loading is well distributed and does not cause widespread high-stress regions. In the added section, the highest compressive stress is recorded under Load Combination 3, with a value of 9.54 MPa (Figure 8). This peak also appears in a localized region near the foundation and crest connections, following a similar pattern to that of the existing section. While slightly higher in magnitude, the stress distribution remains limited in spatial extent, and the overall compressive stress levels are far below the expected compressive strength of mass

concrete, suggesting no risk of crushing or structural compromise.

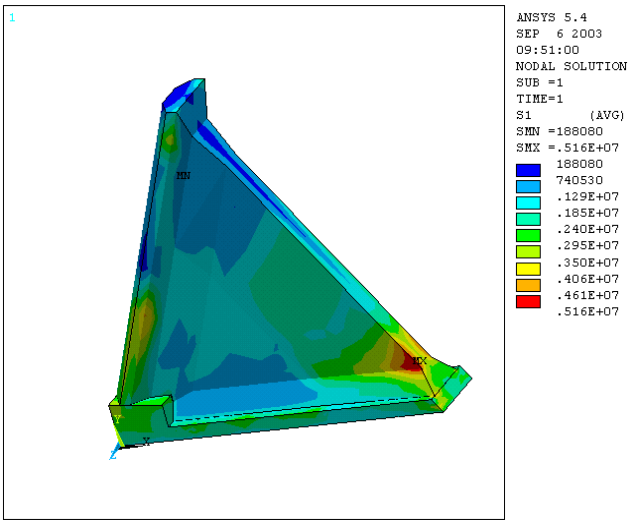

Figure 5. Tensile stress distribution for Load Combination 2 under MCL excitation, localized peaks near the downstream buttress

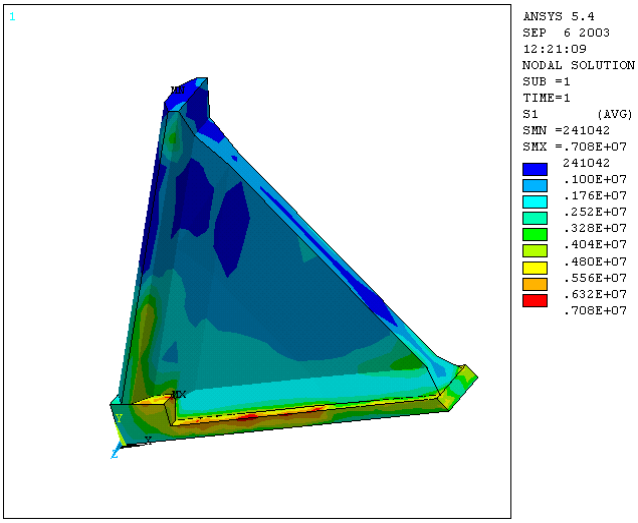

Figure 6. Tensile stress distribution for Load Combination 5 under MCL excitation

Compressive stress peaks are associated with geometric transitions, foundation restraints, and combined hydrodynamic–inertial effects; however, their limited magnitude and extent indicate adequate capacity under MCL loading. In both cases, the concentration of compressive stresses is associated with geometric transitions, foundation restraints, and the combined effects of hydrodynamic and inertial forces under seismic loading. The relatively low magnitudes and localized nature of these peaks confirm that the dam maintains adequate compressive capacity under the considered MCL excitation scenarios.

In summary, the third load combination—comprising the self-weight of the structure, maximum reservoir level, summer thermal condition, and MCL seismic excitation—emerges as the most critical case. This conclusion is supported by the results in Table 9, which show that this combination produces the highest tensile stress at the junction between the added section and the original structure, as well as the most extensive compressive stress distribution, occurring near the dam toe (Zones 5 and 6). Representative displacement contours in the X, Y, and Z directions for this combination are provided in Figures 9 to 11. In this coordinate system, the X-direction corresponds to the longitudinal axis of the dam, the Y-direction to the height of the dam, and the Z-direction to the dam's thickness.

In the X-direction (longitudinal) (Figure 9), the maximum displacement reaches 13.0 mm, occurring at the crest of the dam and oriented toward the downstream side. The displacement increases progressively from the foundation toward the crest, with the most critical zone appearing near the crest at the slope discontinuity, where geometric changes intensify stress and deformation concentration. This pattern reflects the cantilever-type bending response of the dam to longitudinal seismic loading. In the Y-direction (vertical height) (Figure 10), the maximum displacement is 4.5 mm, primarily at the crest region. The displacement contours indicate vertical oscillations along the dam height, with the

base remaining effectively restrained by the foundation. This deformation pattern is consistent with vertical bending and elongation effects induced by seismic motion. In the Z-direction (thickness) (Figure 11), the maximum displacement is 2.3 mm, occurring along the crest and reducing toward the foundation. The pattern shows minor through-thickness deformation, reflecting transverse shear and compression–tension responses caused by the seismic loading. Overall, the displacement magnitudes in all three directions are small compared to the dam dimensions and remain within acceptable safety and serviceability limits, confirming that the dam maintains structural integrity under MCL-level seismic excitation

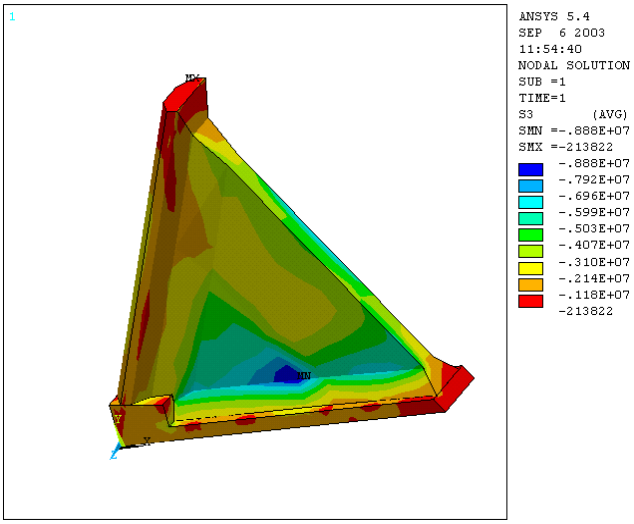

Figure 7. Tensile stress distribution for Load Combination 5 under MCL excitation, localized concentrations at the buttress extremity

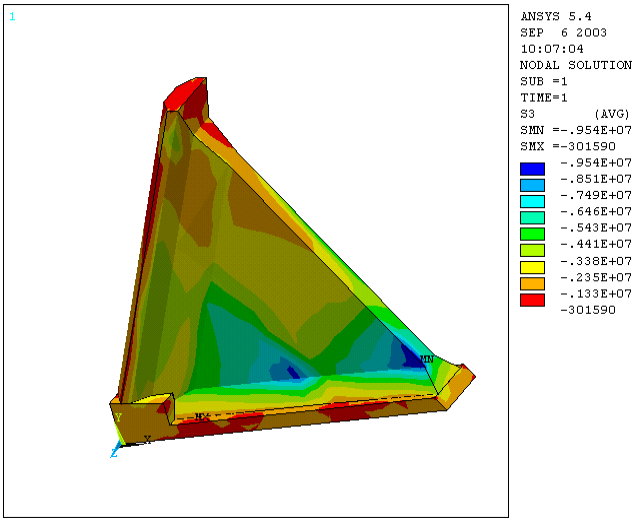

Figure 8. Compressive stress distribution for Load Combination 3 under MCL excitation, localized peaks near the foundation and crest

6. Conclusion

A comprehensive static and seismic evaluation of the proposed 25 m crest heightening of the butress Dam was conducted using three-dimensional finite element modeling, accounting for dam–foundation–reservoir interaction and site-specific loading scenarios. The analysis demonstrated that, for both DBL and MCL seismic levels, maximum tensile and compressive stresses in the existing and added sections are highly localized, primarily near geometric discontinuities, and the downstream buttress ends, and remain well below the concrete's strength capacity. The most critical case, corresponding to Load Combination 3 under MCL excitation, produced a maximum longitudinal crest displacement of 13.0 mm at the slope discontinuity. Yet, this deformation is minimal relative to the dam's dimensions and does not compromise stability. Both static and dynamic responses confirm that the heightened structure maintains adequate safety margins against tensile cracking, compressive crushing, and excessive deformation. The results support the technical feasibility of the heightening project, provided that localized stress concentrations are addressed through appropriate detailing and construction quality control.

While these findings confirm that the heightened dam configuration is safe and technically feasible, they also highlight the importance of addressing localized stress concentrations through practical engineering measures. In

this regard, targeted reinforcement of critical joints, the installation of shear keys at buttress toes, and selective grouting at dam–foundation or dam–addition interfaces may be employed to reduce local stresses further and enhance long-term performance. Such measures can complement the overall design and provide additional assurance for future dam heightening applications.

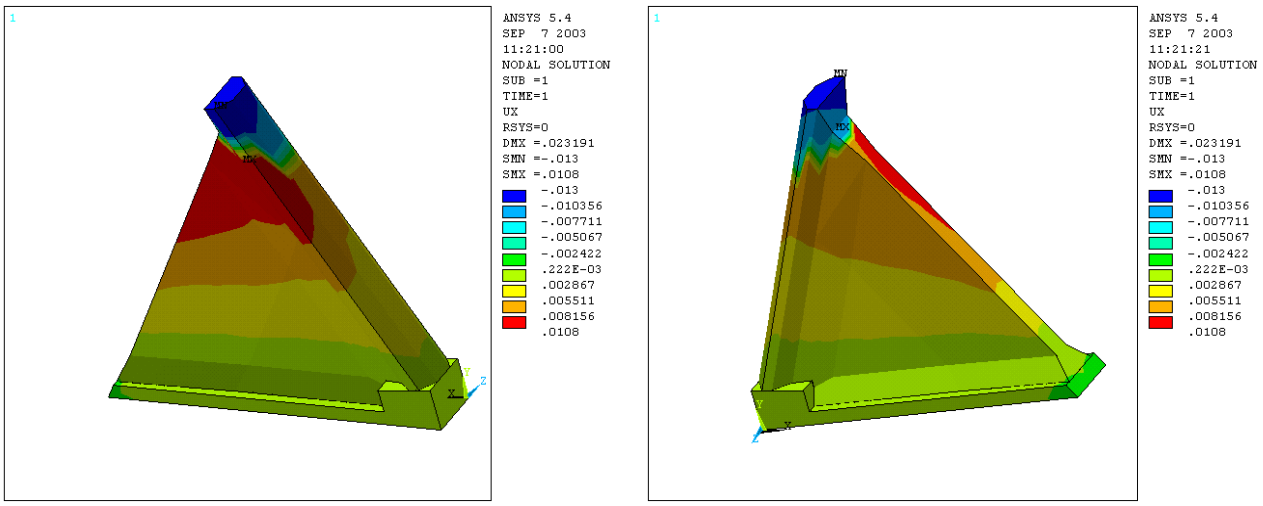

Figure 9. Displacement contours in the X-direction for Load Combination 3 under MCL excitation, showing maximum crest displacement (13 mm)

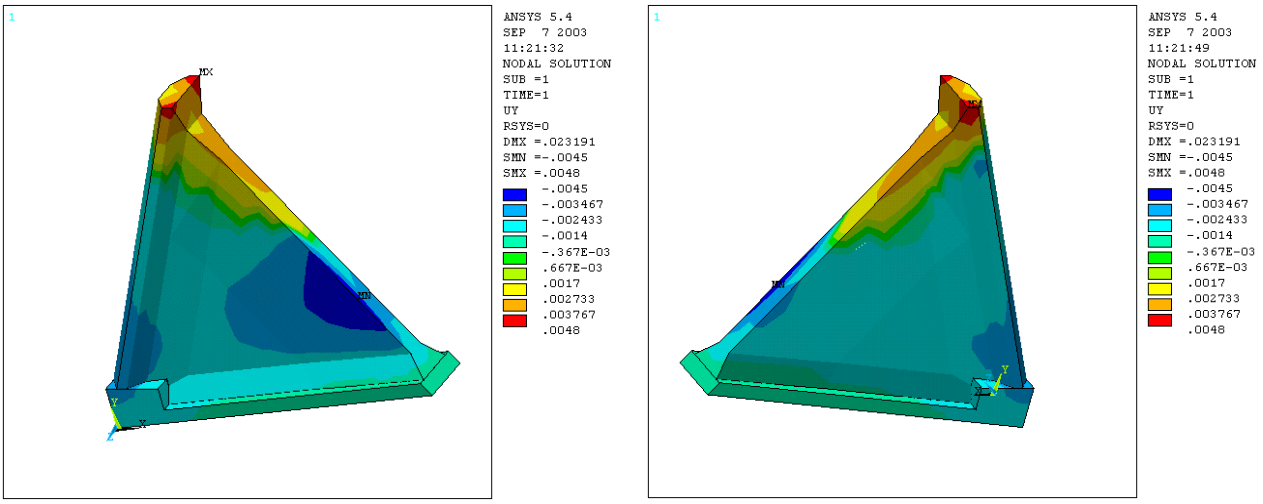

Figure 10. Displacement contours in the Y-direction for Load Combination 3 under MCL excitation, with maximum values at the crest region

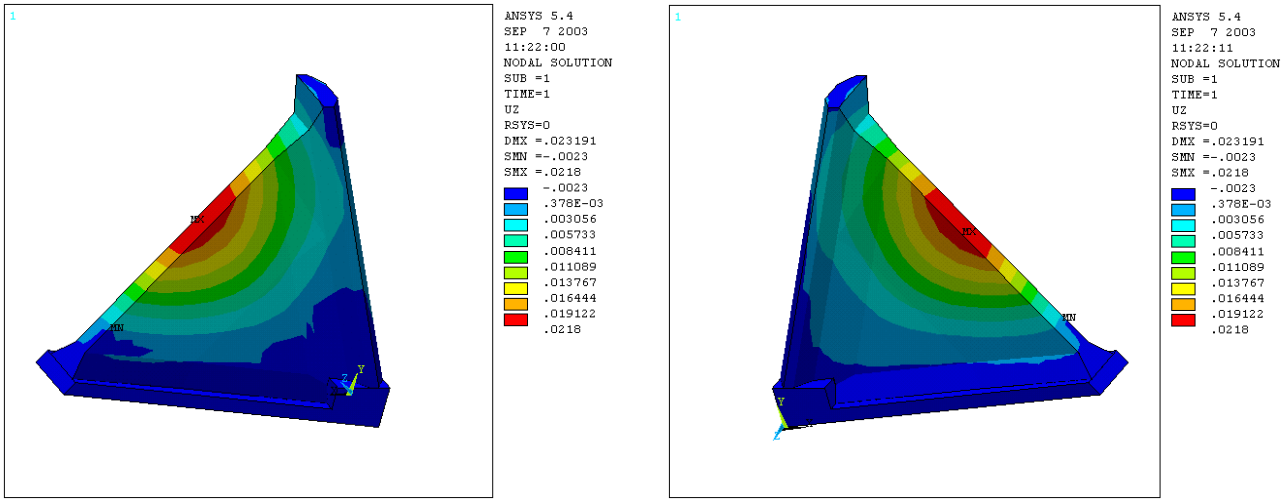

Figure 11. Displacement contours in the Z-direction for Load Combination 3 under MCL excitation, indicating minor through-thickness deformation

6.1. Limitations and Future Work

The analyses presented in this study were conducted under linear-elastic assumptions, which do not explicitly account for nonlinear behavior, such as cracking, joint opening, or sliding, at the dam–foundation interface. Variability in uplift pressure, temperature effects during construction, and material heterogeneity were also not considered. These simplifications are typical for preliminary seismic safety evaluations and provide conservative estimates of structural performance.

Future studies could extend the present work by incorporating nonlinear material models, variable uplift and thermal effects, and long-term monitoring data to validate numerical predictions. Such developments would contribute to a more comprehensive understanding of the seismic and operational performance of heightened buttress dams.

7. References

[1] Ebrahimi Hariri, A., Mohammadi, Y., & Soltani, A. (2025). Numerical simulation of seismic-induced sloshing in rectangular water tanks considering three different approaches. Contributions of Science and Technology for Engineering, 1(4), 16-27. doi:10.22080/cste.2024.28228.1005.

[2] Ghaniyoun, M. H., Moradloo, A., & Asadi, K. N. (2024). Seismic evaluation of concrete gravity dam under the effect of far and near field earthquakes considering dam saturation. Innovative Infrastructure Solutions, 9(9), 356. doi:10.1007/s41062-024-01658-4.

[3] Hussein, T. S., kadir, M. A. A., Alzabeebee, S., & Ramli, M. Z. (2024). Assessing Seismic Vulnerability of Concrete Gravity Dams: A Comparative Analysis of Damage Indexes. Transportation Infrastructure Geotechnology, 11(6), 4061–4097. doi:10.1007/s40515-024-00440-4.

[4] Tanchev, L. (2014). Dams and appurtenant hydraulic structures. CRC Press, Boca Raton, United States.

[5] Dankers, C. L. (2019). A framework for the evaluation of the structural safety of existing concrete gravity dams. Master Thesis, University of Cape Town, Cape Town, South Africa.

[6] Kp, S. S., Shrimali, M. K., Bharati, S. D., & Datta, T. K. (2024). Seismic Performance Evaluation of Concrete Gravity Dams Subjected to Mainshock and Aftershocks. Journal of Vibration Engineering and Technologies, 12(Suppl 2), 1399–1412. doi:10.1007/s42417-024-01481-2.

[7] Zhang, L., Mao, J., & Zhao, L. (2025). Nonlinear Seismic Assessment of Concrete Dams Using a Novel Elastoplastic Damage Numerical Framework. Journal of Engineering Mechanics, 151(4), 4025004. doi:10.1061/jenmdt.emeng-8092.

[8] Mirzabozorg, H., Ghaemian, M., & Aghajanzadeh, S. M. (2020). Static and Dynamic Safety Evaluation of A Heightened Arch Dam Including Massed Foundation Effects. Numerical Methods in Civil Engineering, 4(4), 37–48. doi:10.52547/nmce.4.4.37.

[9] Wohnlich, A., Fankhauser, A., & Feuz, B. (2023). Dam heightening in Switzerland. Role of Dams and Reservoirs in a Successful Energy Transition. CRC Press, Boca Raton, United States.

[10] Ramarao, V. S., & Bhajantri, M. R. (2020). Performance of modified spillway for heightened gravity dam. ISH Journal of Hydraulic Engineering, 26(3), 325–331. doi:10.1080/09715010.2018.1491809.

[11] Feuz, B. (1994). Raising of the Mauvoisin Dam. Structural Engineering International, 4(2), 103–104. doi:10.2749/101686694780650823.

[12] Wieland, M. (2004). Earthquake Safety of Concrete Dams and Seismic Design Criteria for Major Dam Projects. ICOLD publication.

[13] Fu, Z., He, Y., & Su, S. (2011). Key problems and solutions in arch dam heightening. Frontiers of Architecture and Civil Engineering in China, 5(1), 98–104. doi:10.1007/s11709-010-0004-7.

[14] Chen, Y., Gu, C., Wu, B., Shao, C., Wu, Z., & Dai, B. (2019). Inversion Modeling of Dam-Zoning Elasticity Modulus for Heightened Concrete Dam Using ICS-IPSO Algorithm. Mathematical Problems in Engineering, 2019(1), 9328326. doi:10.1155/2019/9328326.

[15] Chen, B., Huang, Z. shen, Bao, T. fei, & Zhu, Z. (2021). Deformation early-warning index for heightened gravity dam during impoundment period. Water Science and Engineering, 14(1), 54–64. doi:10.1016/j.wse.2021.03.001.

[16] Clerc, B., Manso, P., & De Cesare, G. (2021). Heightening of Very High Gravity Dams: The Case Study of the Grande Dixence. Numerical Analysis of Dams. ICOLD-BW 2019. Lecture Notes in Civil Engineering, vol 91. Springer, Cham, Switzerland. doi:10.1007/978-3-030-51085-5_43.

[17] Wang, Y., Yang, H., Zhou, X., & Wu, C. (2016). Study on influence of contact sliding along new-old concrete joint interfaces on gravity dam stability. Journal of Hydroelectric Engineering, 35(3), 121-128. doi:10.11660/slfdxb.20160315.

[18] Kang, F., Liu, J., Li, J., & Li, S. (2017). Concrete dam deformation prediction model for health monitoring based on extreme learning machine. Structural Control and Health Monitoring, 24(10), 1997. doi:10.1002/stc.1997.

[19] Zhu, B. F., Zhang, G. X., Wu, L. K., & Hu, P. (2007). Measures for reducing the cracking of the binding interface between fresh and old concrete in heightening of gravity dam. Journal of hydraulic engineering, 6, 639-645. doi:10.3321/j.issn:0559-9350.2007.06.001

[20] Su, H., Wen, Z., Sun, X., & Yang, M. (2015). Time-varying identification model for dam behavior considering structural reinforcement. Structural Safety, 57, 1–7. doi:10.1016/j.strusafe.2015.07.002.

[21] Sharma, A., Thakur, S., & Nallasivam, K. (2025). Seismic Response Assessment of Concrete Gravity Dam with Dam-Foundation-Reservoir Interaction by Adopting Finite Element Technique. Journal of Vibration Engineering and Technologies, 13(5). doi:10.1007/s42417-025-01905-7.

[22] Rasa, A. Y., Budak, A., & Düzgün, O. A. (2022). An efficient finite element model for dynamic analysis of gravity dam-reservoir-foundation interaction problems. Latin American Journal of Solids and Structures, 19(6). doi:10.1590/1679-78257178.

[23] Habib, A., Al Houri, A., Habib, M., Elzokra, A., & Yildirim, U. (2021). Structural performance and finite element modeling of roller compacted concrete dams: A review. Latin American Journal of Solids and Structures, 18(4). doi:10.1590/1679-78256467.

[24] Karimi, I., Khaji, N., Ahmadi, M. T., & Mirzayee, M. (2010). System identification of concrete gravity dams using artificial neural networks based on a hybrid finite element-boundary element approach. Engineering Structures, 32(11), 3583–3591. doi:10.1016/j.engstruct.2010.08.002.

[25] Zhang, S., Wang, G., & Yu, X. (2013). Seismic cracking analysis of concrete gravity dams with initial cracks using the extended finite element method. Engineering Structures, 56, 528–543. doi:10.1016/j.engstruct.2013.05.037.

[26] Løkke, A., & Chopra, A. K. (2019). Direct finite element method for nonlinear earthquake analysis of concrete dams: Simplification, modeling, and practical application. Earthquake Engineering and Structural Dynamics, 48(7), 818–842. doi:10.1002/eqe.3150.

[27] Mahdian Khalil, A., & Navayi Neya, B. (2025). Seismic Analysis of Concrete Buttress Dam Considering Intake Tower and Reservoir. Journal of Rehabilitation in Civil Engineering, 13(1), 130–150. doi:10.22075/jrce.2024.31734.1897.

[28] Enzell, J., Nordström, E., Sjölander, A., Ansell, A., & Malm, R. (2023). Physical Model Tests of Concrete Buttress Dams with Failure Imposed by Hydrostatic Water Pressure. Water, 15(20), 3627. doi:10.3390/w15203627

[29] Abbasiverki, R., Malm, R., Ansell, A., & Nordström, E. (2021). Nonlinear Behaviour of Concrete Buttress Dams under High-Frequency Excitations Taking into Account Topographical Amplifications. Shock and Vibration, 2021(1). doi:10.1155/2021/4944682.

[30] Aghajanzadeh, S. M., & Ghaemian, M. (2013). Nonlinear dynamic analysis of a concrete gravity dam considering an elastoplastic constitutive model for the foundation. Scientia Iranica, 20(6), 1676–1684.